JOURNAL OF AIRCRAFT
Vol. 45, No. 2, March–April 2008

Approximate Internal Load Prediction in Composite Structures with Locally Buckled Panels

Omprakash Seresta*
Virginia Polytechnic Institute State University, Blacksburg, Virginia 24061
and
Mostafa M. Abdalla† and Zafer Gürdal‡
Delft University of Technology, 1-2629 HS Delft, The Netherlands

DOI: 10.2514/1.30465

Most aerospace structural designs are complex assemblies of a large number of panel components. In designing such a structure, it is customary to divide the structure into many regions and design them independently/semi-independently. A coarse finite element model of the entire structure is first used to determine loads in each component, and subsequently the components are designed using local constraints and performance requirements for these fixed loads. This two-level approach works well if a linear static behavior is considered. For cases in which local components display postbuckling behavior, the internal load distribution in the structure is altered requiring nonlinear global analysis, which is computationally expensive. This paper focuses on developing a computationally efficient approximate methodology for predicting internal load distribution in a structure considering some or all panels to be buckled. In this paper, a semi-analytical approach based on the Rayleigh–Ritz method and the perturbation approach is developed to compute the postbuckled stiffness of buckled panels. An iterative procedure is suggested to predict the internal load distribution with successive buckling during loading. Three different examples are presented. A simply supported flat composite panel subjected to different edge compression is used to verify the perturbation approach used for the calculation of the postbuckled panel stiffness. A two-panel arrangement with different thicknesses subjected to end compression and a 48-panel composite wing structure subjected to bending load are used as cases for structures with buckled panel components. In all cases, the present approach agrees with full nonlinear analysis in predicting the internal load distribution.

Nomenclature

A_{ij}	=	in-plane stiffness coefficients
A_{ij}^{PB}	=	postbuckled stiffness coefficients
$\underline{a}$, $\underline{b}$	=	dimension of the plate in the x and y directions, respectively
$a_i^{(0)}, a_i^{(1)}, \ldots$	=	terms in expansion of a_i
b_i, c_i, a_i	=	Ritz coefficients associated with u, v, and w, respectively
D_{ij}	=	bending stiffness coefficients
e_{x0}, e_{y0}, g_{xy0}	=	applied edge strains
e_{x0}^k, e_{y0}^k, g_{xy0}^k	=	applied average strains e_{x0}, e_{y0}, g_{xy0} at the kth step of the approximate internal load prediction scheme
$e_{x0}^{(0)}, e_{x0}^{(1)}, \ldots$	=	terms in expansion of e_{x0}
$e_{y0}^{(0)}, e_{y0}^{(1)}, \ldots$	=	terms in expansion of e_{y0}
g_l^u, g_l^v	=	first-order tensor coefficients in equilibrium equations
g_l^{ux}, g_l^{uy}, g_l^{uxy}	=	components of g_l^u
g_l^{vx}, g_l^{vy}, g_l^{vxy}	=	components of g_l^v
$g_{xy0}^{(0)}, g_{xy0}^{(1)}, \ldots$	=	terms in expansion of g_{xy0}
K_b	=	reduced tangential stiffness matrix of any panel in the structure at the kth step of the approximate internal load prediction scheme
K_{ij}	=	linear stiffness matrix coefficients
K_{ij}^g	=	geometric stiffness matrix coefficients
K_{ijkl}^{NL}	=	fourth-order nonlinear tensor coefficients
K_{ijkl}^{waaa}	=	fourth-order tensor coefficients in equilibrium equation associated with w
K_{ijl}^{uaa}	=	third-order tensor coefficients in equilibrium equation associated with u
K_{ijl}^{vaa}	=	third-order tensor coefficients in equilibrium equation associated with v
K_{ikl}^{wba}, K_{ikl}^{wca}	=	third-order tensor coefficients in equilibrium equation associated with w
$\bar{K}_{il}^g$	=	second-order tensor coefficients in equilibrium equation associated with w
$\bar{K}_{il}^{gx}$, $\bar{K}_{il}^{gy}$, $\bar{K}_{il}^{gxy}$	=	components of $\bar{K}_{il}^g$
K_{il}^{gx}, K_{il}^{gy}, K_{il}^{gxy}	=	components of K_{il}^g
K_{il}^{ub}, K_{il}^{uc}	=	second-order tensor coefficients in equilibrium equation associated with u
K_{il}^{vb}, K_{il}^{vc}	=	second-order tensor coefficients in equilibrium equation associated with v
m, n	=	number of terms in a double sine series
N	=	total number of terms in a double sine series
N_s, N_n	=	applied load along s and normal to s, respectively
N_x, N_y, N_{xy}	=	average load along the edges
$\bar{N}_x$, $\bar{N}_y$, $\bar{N}_{xy}$	=	average loads defined in the edge displacement loaded edges
s	=	contour direction along the perimeter of the plate or domain
u, v, w	=	displacement along the x, y, and z directions, respectively
u_s, u_n	=	displacement along s and normal to s, respectively
u_0, v_0	=	applied edge displacements
$\Delta\lambda$	=	buckling factor of any panel in the structure at the kth step of the approximate internal load prediction scheme

Received 14 February 2007; revision received 5 September 2007; accepted for publication 31 October 2007.

*Research Assistant, Department of Aerospace and Ocean Engineering, 215 Randolph Hall; oseresta@vt.edu. Student Member AIAA.

†Assistant Professor, Aerospace Structures, Kluyverweg; m.m.abdalla@tudelft.nl. Member AIAA.

‡Professor, Aerospace Structures, Kluyverweg; z.gurdal@tudelft.nl. Associate Fellow AIAA.

$\Delta\lambda^k$	=	incremental load factor at the kth step of the approximate internal load prediction scheme
$\epsilon_x, \epsilon_y, \gamma_{xy}$	=	strains
$\epsilon_x^0, \epsilon_y^0, \gamma_{xy}^0$	=	midplane strains
$\kappa_x, \kappa_y, \kappa_{xy}$	=	curvatures
λ	=	load scaling factor
λ^k	=	total load applied at the kth step of the approximate internal load prediction scheme
Π	=	total potential
Φ	=	external virtual work
$\phi_i^u, \phi_i^v, \phi_i^w$	=	assumed modes in Rayleigh–Ritz for u, v, and w, respectively

I. Introduction

THE design of complex built-up structures requires the design of the local details of all subcomponents. An example is the design of an aircraft fuselage, which is made up of several stiffened panels. Here, the local design variables are stiffener spacing or positions, stiffener dimensions, panel skin thickness, etc. Another example is the design of a wing structure configuration in which the local design variables, among others, are ribs, spars or skin panel thickness, and skin stiffener spacing and dimensions. In the case of composite structures, these local details include the stacking sequence of laminates and ply compositions if two or more types of materials are used. With such a wide range of design variables, design can be difficult or computationally expensive. Furthermore, many response functions that are used in design optimization require a complete analysis of the entire structure under specified design loads. Full-scale analysis of structures using detailed finite element models with a large number of degrees of freedom is computationally expensive. When such analysis models are coupled with an optimizer, which necessitates repetitive analysis, the computational cost of the design optimization becomes prohibitively expensive and may exceed the limits of present computational capabilities. To reduce the computational effort while maintaining high fidelity analyses, various modeling approaches and improvements to the design methodologies are used.

One approach to reduce complexity in a large scale design optimization problem is to decompose the problem into several smaller independent/semi-independent design optimization problems and a coordination problem to preserve coupling and/or compatibility among these subproblems. This multilevel approach makes the big problem more manageable and tractable. The decomposition also favors simultaneous work on different parts of the problem, which significantly reduces the product development time. The general multilevel approach is to divide the system into a hierarchy of subsystems. For example, in a multilevel design of aircraft structures, the structure is divided into panels or regions that may be designed independently or semi-independently.

Most of the earlier attempts of such formulations were based on the fully stressed design (FSD) concept. The FSD technique implies that material is removed from structural components unless minimum thickness constraints are violated or the structure is stressed to its maximum for the given failure criterion under the specified loading condition. Lansing et al. [1] and Giles [2] have used this method extensively for aerospace structures. Sobieszczanski-Sobieski and Leondorf [3] developed a multilevel optimization procedure for the design of a fuselage structure. The structure is designed in two stages. First, an overall material distribution is found by applying the FSD technique to an idealized model of the structure. Second, the detailed design of the structural subcomponents is performed by mathematical optimization. Schmit and Ramanathan [4] proposed a modified version of this approach to avoid some numerical difficulties associated with continuous optimization. Schmit and Mehrinfar [5] also successfully extended the multilevel approach to the design of composite structures. Sobieszczanski-Sobieski et al. [6,7] later proposed a generalized multilevel approach. The decomposition is achieved by separating the structural element optimization problem from the assembled structural optimization problem. Equality constraints at the subsystem level are imposed to maintain model compatibility between the system and subsystem levels. Ragon et al. [8] demonstrated a global/local design methodology for the wing structure design problem. Liu et al. [9] employed a similar two-level design approach using genetic algorithms and response surfaces for a composite wing structure design problem.

One of the important steps in multilevel structural design is to predict the internal load distribution in the structure, which is commonly referred to as the load path. The importance stems from the fact that these internal loads dictate the dimensions of the structural subcomponents being designed. Conversely, the local dimensions and details affect the internal load distribution creating interdependency. To compute the internal loads (load paths), highly idealized and simplified global models are often used because of the computational cost involved with a full-scale detailed analysis of a large structure. For example, at the preliminary stage of a fuselage or wing design, each panel between stiffeners or ribs or spars is modeled via a single element to avoid the computational overhead associated with a full-scale detailed finite element analysis. The aim of the global analysis is to then determine the internal load distribution. This is the reason that the global model is also commonly referred to as the loads model. Based on these internal loads, the subcomponents are designed against strain, stability or buckling, and manufacturing constraints.

Thus, the research focus in multilevel structural design procedures can be classified into two areas: first, the development of a loads model with a reasonable number of degrees of freedom for complex structures so that it can be used in optimization studies; and second, the development of cheap local models (usually a simple structural component, such as a beam, panel, etc.) to be used in local detailing. In the last four decades, the research focus was mainly on developing faster, cheaper, and accurate local models. A comprehensive literature exists on the analysis and design optimization of composite components against buckling [10–15], postbuckling [16–20], and failure. Note that these references are not exhaustive in nature.

In thin-walled structures, one of the most important local modes of failure is the buckling of a component panel. After buckling, the load carrying capacity of the panel is reduced because of reduced stiffness. In practice, however, it is customary to allow the secondary load carrying components (such as the skin panels of a fuselage) to carry loads beyond their buckling load while the overall structure can be further loaded. The multilevel approach already discussed is limited by the capabilities of the loads model to predict accurately the internal load distribution. In the case of a structure with locally buckled panels, an idealized loads model based on a linear finite element analysis fails to capture the change in local stiffness. This could be rectified by using a detailed nonlinear loads model, which is computationally expensive. Hence, there is a need for a cheap and sufficiently accurate procedure to predict internal loads in structures with buckled components.

Grisham [21] proposed a methodology for a metallic structure to incorporate the reduced load carrying capacity of a buckled component by applying prestrains. However, Grisham's algorithm requires a detailed mesh of the components and as such it is not suitable as a loads model. A computer program for the design of plate assemblies based on initial buckling called VICONOPT [22] was modified by Anderson [23] to allow for a limited postbuckling capability. This is achieved by reducing the overall stiffness of a buckled plate by an arbitrary factor chosen as 2. Viljoen et al. [24] implemented Grisham's algorithm for the design of stiffened thin-walled panels in shear. An ad hoc approach was used by Collier et al. [25] to account for the local postbuckling of skins by forcing the analysis module to disregard the already buckled portion of the skin such that it carries no additional load. This is achieved by reducing the effective width of the component. A similar approach was proposed by Haftka [26], in which it is assumed that a component carries no additional load after buckling. Another approach that is being explored currently is to replace the global loads model of the structure with a response surface [27,28]. In both of these works, only the axial load is considered and the design space is kept small enough to facilitate the construction of surrogate models. A nonlinear

idealization of structures with axial loads was proposed by Murphy et al. [29]. Their work is based on representing each component by a single one-dimensional nonlinear spring element in the global model. A number of detailed finite element analyses of the components are performed a priori to generate the spring data. This method also comes into the purview of response surface methods, though it does not use response surfaces directly to model the global loads model response, but only to generate the spring data. Moreover, this methodology cannot be easily extended to biaxially loaded structures or structures under more complicated loading cases, such as a wing structure under bending loads. Recently, Kling et al. [30] developed a hybrid subspace analysis procedure for the nonlinear static analysis of beam-type structures. In this work, the buckling modes and path derivatives have been used as global shape functions to reduce the conventional full finite element system. This approach, though it reduces the computational cost compared with the full nonlinear analysis, is still too expensive to be employed as a loads model. Moreover, this methodology has not been extended to plate structures.

In all of the aforementioned literature, except in the field of surrogate approximation, only metallic (isotropic) structures are considered. To the authors' knowledge, no work to quantify the response of locally buckled panels is performed for composite structures. The motivating factor of the current work can be best described by the following quote from Grisham's [21] original paper: "A generalized method does not yet exist for predicting reliably the postbuckling moduli of plates." This paper focuses on developing a general methodology to predict the approximate internal load distribution (load paths) in a composite structure with buckled local panels. After buckling, though the stiffness of the panel is reduced, the load response is assumed to be essentially linear. This assumption is valid if the panel is not loaded too deeply into the postbuckling regime. In the first section of the paper, the postbuckled stiffness of a simply supported buckled laminate is derived using a perturbation approach. Next, an iterative procedure is proposed to predict the internal loads in a postbuckled structure with multiple locally buckled panels. At each step in the proposed methodology, a linear global finite element analysis is performed using an idealized linear loads model. This approach reduces the number of degrees of freedom in the finite element model significantly compared with a nonlinear analysis.

The rest of the paper is organized as follows: the reduced stiffness modeling of a postbuckled panel is provided in Sec. II, the internal load prediction scheme is described in Sec. III, followed by results in Sec. IV, and conclusions in Sec. V.

II. Reduced Stiffness Modeling

Consider a laminate of dimensions $\underline{a} \times \underline{b}$ (Fig. 1) subjected to an edge displacement at $x = \underline{a}$ and $y = \underline{b}$. Assuming that the plate is thin, such that the Kirchhoff hypothesis is valid, the strain in terms of midplane strains (superscript 0) are given as [31–33]

$$\epsilon_x = \epsilon_x^0 + z\kappa_x, \qquad \epsilon_y = \epsilon_y^0 + z\kappa_y, \quad \text{and} \quad \gamma_{xy} = \gamma_{xy}^0 + z\kappa_{xy} \tag{1}$$

For moderately large rotations, following the von Kármán model, midplane strains and curvature terms are given in terms of midplane displacements u, v, and w as [31–33]

$$\begin{aligned}
\epsilon_x^0 &= u_{,x} + \tfrac{1}{2}w_{,x}^2,\\
\epsilon_y^0 &= v_{,y} + \tfrac{1}{2}w_{,y}^2,\\
\gamma_{xy}^0 &= u_{,y} + v_{,x} + w_{,x}w_{,y},\\
\kappa_x &= -w_{,xx}, \kappa_y = -w_{,yy},\\
\kappa_{xy} &= -2w_{,xy}
\end{aligned} \tag{2}$$

where a comma with a variable following it in the subscript indicates the space derivative with respect to that variable.

The total potential, using the expression of strain in Eq. (2), of a symmetric and a balanced laminate is given by [31–33]

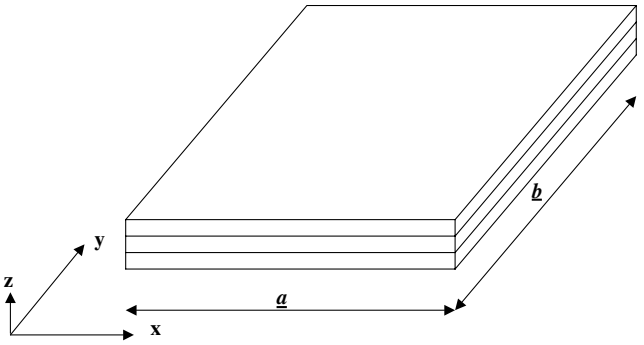

Fig. 1 Flat composite panel.

$$\begin{aligned}
\Pi(u, v, w) = \frac{1}{2}\int_0^{\underline{a}}\int_0^{\underline{b}} &[A_{11}(\epsilon_x^0)^2 + 2A_{12}\epsilon_x^0\epsilon_y^0 + A_{22}(\epsilon_y^0)^2\\
&+ A_{66}(\gamma_{xy}^0)^2 D_{11}\kappa_x^2 + 2D_{12}\kappa_x\kappa_y + D_{22}\kappa_y^2 + D_{66}\kappa_{xy}^2]\,\mathrm{d}x\,\mathrm{d}y
\end{aligned} \tag{3}$$

where the in-plane stiffness coefficients, A_{11}, A_{12}, A_{22}, and A_{66}, and the flexural stiffness coefficients, D_{11}, D_{12}, D_{22}, and D_{66}, are given in terms of the engineering constants of the materials and the laminate stacking sequence [32]. The bending twisting terms D_{16} and D_{26} are neglected. Extending the formulation to unbalanced laminates is straightforward and will not be discussed.

Following Rayleigh–Ritz procedure [34], displacement functions are assumed in the form of

$$\begin{aligned}
w(x, y) &= \sum_{i=1}^{N} a_i\phi_i^w,\\
u(x, y) &= -\lambda e_{x0}x - \lambda\frac{g_{xy0}}{2}y + \sum_{i=1}^{2N} b_i\phi_i^u, \quad \text{and}\\
v(x, y) &= -\lambda e_{y0}y - \lambda\frac{g_{xy0}}{2}x + \sum_{i=1}^{2N} c_i\phi_i^v
\end{aligned} \tag{4}$$

where λ is the scaling factor associated with applied edge strains e_{x0}, e_{y0}, and g_{xy0}. Note that the number of assumed modes for in-plane displacements u and v is twice that of transverse displacement w. This is done to ensure that the in-plane equilibrium is adequately satisfied based on the authors' previous experience [18]. Depending on the choice of assumed modes ϕ_i^u, ϕi^v, and ϕ_i^w, different boundary conditions can be modeled. In this work, simply supported boundary conditions are considered and a double sine series for ϕ_i^u, ϕ_i^v, and ϕ_i^w is assumed

$$\phi_i^{u/v/w} = \mathrm{Sin}\frac{m\pi x}{\underline{a}}\mathrm{Sin}\frac{n\pi y}{\underline{b}} \tag{5}$$

where m and n are integers that vary from $1, 2, \ldots, M$, in which M indicates the number of terms in either direction, therefore yielding a total of $N = M^2$ terms in the series. Therefore, i is expressed as $i = M(m-1) + n$. Note that, although in the current study we assumed the number of terms in u and v to be equal and used the same number of half sine waves in both the x and y directions, this does not limit the approximate methodology. Based on one's own experience, one can judiciously assign a different number of terms depending on the problem.

The edge displacements u_0 at the edge $x = \underline{a}$, and v_0 at the edge $y = \underline{b}$, are expressed in terms of the applied edge strains as

$$u_0 = e_{x0}\underline{a} + \frac{g_{xy0}}{2}y, \qquad v_0 = e_{y0}\underline{b} + \frac{g_{xy0}}{2}x \tag{6}$$

This applied edge displacement guarantees that the plate edges remain straight after deformation, which is a reasonable idealization of skin panels commonly used in stiffened aerospace structures. The boundary conditions follow from the fact that the adjacent structural components and stiffeners are exerting resistance to deformation, as

in the case of a composite wing structure design [18]. Note that e_{x0}, e_{y0}, and g_{xy0} control the applied displacement loading and are not the actual midplane strains. They represent the average strain over the laminate. For example, in the absence of g_{xy0}, e_{x0} is equal to $u_0/\underline{a}$.

By minimizing the total potential with respect to the Ritz coefficients a_i, b_i, and c_i, we obtain the general equilibrium equation for a symmetric and balanced laminated composite plate (see Appendix A for the definition of the tensors in the following equations):

$$\begin{aligned} &-g_l^u + K_{il}^{ub} b_i + K_{il}^{uc} c_i + K_{ijl}^{uaa} a_i a_j = 0, \\ &-g_l^v + K_{il}^{vb} b_i + K_{il}^{vc} c_i + K_{ijl}^{vaa} a_i a_j = 0, \\ &K_{il} a_i - \lambda \bar{K}_{il}^{g} a_i + K_{ikl}^{wba} b_i a_k + K_{ikl}^{wca} c_i a_k + K_{ijkl}^{waaa} a_i a_j a_k = 0 \end{aligned} \tag{7}$$

where

$$\begin{aligned} g_l^u &= g_l^{ux} e_{x0} + g_l^{uy} e_{y0} + g_l^{uxy} g_{xy0} \\ g_l^v &= g_l^{vx} e_{x0} + g_l^{vy} e_{y0} + g_l^{vxy} g_{xy0} \\ \bar{K}_{il}^{g} &= \bar{K}_{il}^{gx} e_{x0} + \bar{K}_{il}^{gy} e_{y0} + \bar{K}_{il}^{gxy} g_{xy0} \end{aligned} \tag{8}$$

The first two equations in Eq. (7) are linear in the Ritz coeffcients corresponding to in-plane displacement. Thus, the preceding three equations can be reduced to a single nonlinear equation by eliminating the b_i and c_i coefficients from the last equation. For details of this condensation procedure, the reader is referred to Appendix B. The final nonlinear equation obtained after condensation is

$$[K_{il} - \lambda K_{il}^{g}] a_i + K_{ijkl}^{\mathrm{NL}} a_i a_j a_k = 0 \tag{9}$$

where

$$K_{il}^{g} = K_{il}^{gx} e_{x0} + K_{il}^{gy} e_{y0} + K_{il}^{gxy} g_{xy0} \tag{10}$$

One of the important steps in the current formulation is to define average loads in the postbuckled regime. The external virtual work is defined as

$$\Phi = \int_0^S (N_s \delta u_s + N_n \delta u_n)\, \mathrm{d}s \tag{11}$$

where s is the contour direction taken along the perimeter of the plate in a counterclockwise direction and n is the outward normal direction to the contour defined by s. S is the total length or perimeter of the contour, N_s is the load along the tangential direction to s, and N_n is the load along the normal direction to n. After taking the boundary conditions into consideration and substituting the different expressions, we get the following form:

$$\begin{aligned} \Phi = &\left[\underline{a} \int_0^{\underline{b}} N_x(\underline{a}, y)\, \mathrm{d}y - \int_0^{\underline{a}} N_{xy}(x, 0) x dx \right. \\ &\left. + \int_0^{\underline{a}} N_{xy}(x, \underline{b}) x dx \right] (-e_{x0}) \\ &+ \left[\underline{b} \int_0^{\underline{a}} N_y(x, \underline{b})\, \mathrm{d}x - \int_0^{\underline{b}} N_{xy}(0, y) y\, \mathrm{d}y \right. \\ &\left. + \int_0^{\underline{b}} N_{xy}(\underline{a}, y) y\, \mathrm{d}y \right] (-e_{y0}) \\ &+ \left[\frac{1}{2} \int_0^{\underline{b}} N_x(\underline{a}, y) y\, \mathrm{d}y + \frac{1}{2} \int_0^{\underline{a}} N_y(x, \underline{b}) x\, \mathrm{d}x \right. \\ &\left. + \frac{\underline{a}}{2} \int_0^{\underline{b}} N_{xy}(\underline{a}, y)\, \mathrm{d}y + \frac{\underline{b}}{2} \int_0^{\underline{a}} N_{xy}(x, \underline{b})\, \mathrm{d}x \right] (-g_{xy0}) \\ &= [\bar{N}_x(-e_{x0}) + \bar{N}_y(-e_{y0}) + \bar{N}_{xy}(-g_{xy0})](\underline{a}\underline{b}) \end{aligned} \tag{12}$$

where $\bar{N}_x$, $\bar{N}_y$, and $\bar{N}_{xy}$ are the average in-plane stress resultants.

The in-plane initial postbuckled stiffness coefficients are then defined by the following expressions:

$$\begin{aligned} A_{11}^{\mathrm{PB}} &= \frac{D\bar{N}_x}{De_{x0}}; \qquad A_{12}^{\mathrm{PB}} = \frac{D\bar{N}_x}{De_{y0}} \\ A_{21}^{\mathrm{PB}} &= \frac{D\bar{N}_y}{De_{x0}}; \qquad A_{22}^{\mathrm{PB}} = \frac{D\bar{N}_y}{De_{y0}} \\ A_{66}^{\mathrm{PB}} &= \frac{D\bar{N}_{xy}}{Dg_{xy0}} \end{aligned} \tag{13}$$

where the derivatives are to be evaluated at the buckling point. Because at bifurcation (buckling) point the equilibrium equations are singular, precluding a formal chain rule evaluation of the derivatives, we employ a perturbation technique to compute the initial postbuckled in-plane stiffness coefficients.

The nonlinear equilibrium equation Eq. (9) depends on the following parameters: e_{x0}, e_{y0}, g_{xy0}, and a_i. Each of these parameters is expanded in terms of a small parameter ϵ that measures perturbation from values at the buckling point as follows:

$$\begin{aligned} e_{x0} &= e_{x0}^{(0)} + \epsilon^2 e_{x0}^{(2)} + \cdots \qquad e_{y0} = e_{y0}^{(0)} + \epsilon^2 e_{y0}^{(2)} + \cdots \\ g_{xy0} &= g_{xy0}^{(0)} + \epsilon^2 g_{xy0}^{(2)} + \cdots \qquad a_i = \epsilon a_i^{(1)} + \epsilon^3 a_i^{(3)} + \cdots \end{aligned} \tag{14}$$

Note that the zeroth order terms in these expressions correspond to the prebuckling state and hence $a_i^{(0)} = \{0\}$. Also $a_i^{(1)}$ corresponds to the buckling state, and hence in-plane terms $e_{x0}^{(1)}$ vanish and in the postbuckling region only third-order nonlinearity corresponding to a_is exist. This can be easily verified by substituting the complete expansion and equating the corresponding ϵ terms.

Substituting the preceding expressions into Eq. (9) and comparing the coefficients of ϵ gives the linear buckling eigenvalue problem from which we can determine the critical values of the applied strain levels $e_{x0}^{(0)}$, $e_{y0}^{(0)}$, and $g_{xy0}^{(0)}$ and the corresponding buckling mode $a_i^{(1)}$. Comparing the coefficients of ϵ^3, we obtain the following equation:

$$\begin{aligned} &K_{il} a_i^{(3)} - K_{il}^{gx} a_i^{(3)} e_{x0}^{(0)} - K_{il}^{gy} a_i^{(3)} e_{y0}^{(0)} - K_{il}^{gxy} a_i^{(3)} g_{xy0}^{(0)} \\ &\quad = K_{il}^{gx} a_i^{(1)} e_{x0}^{(2)} + K_{il}^{gy} a_i^{(1)} e_{y0}^{(2)} + K_{il}^{gxy} a_i^{(1)} g_{xy0}^{(2)} + K_{ijkl}^{\mathrm{NL}} a_i^{(1)} a_j^{(1)} a_k^{(1)} \end{aligned} \tag{15}$$

The equation for $a_i^{(3)}$ is singular and the solvability condition requires

$$\begin{aligned} &K_{il}^{gx} a_i^{(1)} a_l^{(1)} e_{x0}^{(2)} + K_{il}^{gy} a_i^{(1)} a_l^{(1)} e_{y0}^{(2)} + K_{il}^{gxy} a_i^{(1)} a_l^{(1)} g_{xy0}^{(2)} \\ &\quad + K_{ijkl}^{\mathrm{NL}} a_i^{(1)} a_j^{(1)} a_k^{(1)} a_l^{(1)} = 0 \end{aligned} \tag{16}$$

From this equation, a unique relation has to be satisfied by the second-order perturbation coefficients $e_{x0}^{(2)}$, $e_{y0}^{(2)}$, and $g_{xy0}^{(2)}$. For the calculation of the postbuckled panel stiffness, we need to vary the average applied strains (e_{x0}, e_{y0}, and g_{xy0}) independently. Thus, we determine the value of each of the second-order coefficients when the other two are assigned zero values. These values can be calculated from Eq. (16) as

$$e_{x0}^{(2)} = \frac{K_{ijkl}^{\mathrm{NL}} a_i^{(1)} a_j^{(1)} a_k^{(1)} a_l^{(1)}}{K_{il}^{gx} a_i^{(1)} a_l^{(1)L}} \tag{17}$$

$$e_{y0}^{(2)} = \frac{K_{ijkl}^{\mathrm{NL}} a_i^{(1)} a_j^{(1)} a_k^{(1)} a_l^{(1)}}{K_{il}^{gy} a_i^{(1)} a_l^{(1)}} \tag{18}$$

$$g_{xy0}^{(2)} = \frac{K_{ijkl}^{\mathrm{NL}} a_i^{(1)} a_j^{(1)} a_k^{(1)} a_l^{(1)}}{K_{il}^{gxy} a_i^{(1)} a_l^{(1)}} \tag{19}$$

The average in-plane stress resultants, $\bar{N}_x$, $\bar{N}_y$, and $\bar{N}_{xy}$, are also expanded in terms of perturbation parameter ϵ as

$$\bar{N}_x = \bar{N}_x^{(0)} + \epsilon^2 \bar{N}_x^{(2)} + \cdots$$
$$\bar{N}_y = \bar{N}_y^{(0)} + \epsilon^2 \bar{N}_y^{(2)} + \cdots$$
$$\bar{N}_{xy} = \bar{N}_{xy}^{(0)} + \epsilon^2 \bar{N}_{xy}^{(2)} + \cdots \tag{20}$$

The determination of this expansion is straightforward because the average in-plane resultants are uniquely defined by the displacements and average strains. Please note that only second-order nonlinearity exists.

Now the approximate postbuckled stiffness can be computed by taking the ratio of the leading variations of average in-plane stress resultants to the leading variations in average in-plane strains, which results in the following expressions:

$$A_{11}^{\mathrm{PB}} = \frac{\bar{N}_x^{(2)}}{e_{x0}^{(2)}}; \qquad A_{12}^{\mathrm{PB}} = \frac{\bar{N}_x^{(2)}}{e_{y0}^{(2)}};$$
$$A_{21}^{\mathrm{PB}} = \frac{\bar{N}_y^{(2)}}{e_{x0}^{(2)}}; \qquad A_{22}^{\mathrm{PB}} = \frac{\bar{N}_y^{(2)}}{e_{y0}^{(2)}};$$
$$A_{66}^{\mathrm{PB}} = \frac{\bar{N}_{xy}^{(2)}}{g_{xy0}^{(2)}} \tag{21}$$

In general, the terms A_{12}^{PB} and A_{21}^{PB} are not numerically the same and the approximate postbuckling stiffness matrix is not symmetric. Symmetry is asymptotically approached as the number of terms in the Rayleigh–Ritz expansion is increased.

III. Internal Load Prediction Scheme

In this section, we present a general approach to predicting the internal load distribution in an assembled structure in which some or all panels are allowed to go into the postbuckling regime. The internal load prediction scheme consists of the following steps:

1) Set the step number $k = 0$. Initialize the average strains of all panels ($e_{x0}^0 = 0$, $e_{y0}^0 = 0$, and $g_{xy0}^0 = 0$) and the load control factor $\lambda^0 = 0$. Initialize all panel stiffness to their linear (classical lamination) values.

2) Perform a linear finite element analysis to compute the internal load distribution in the structure and recover the average strains of each panel. These average strains are denoted by Δe_{x0}, Δe_{y0}, and Δg_{xy0}.

Consistent with the local postbuckling model, the average strain variation with load is assumed to be piecewise linear. Thus, the actual average strains in any panel are given by

$$e_{x0}^{k+1} = e_{x0}^k + \Delta\lambda^{k+1}\Delta e_{x0}^{k+1}$$
$$e_{y0}^{k+1} = e_{y0}^k + \Delta\lambda^{k+1}\Delta e_{y0}^{k+1}$$
$$g_{xy0}^{k+1} = g_{xy0}^k + \Delta\lambda^{k+1}\Delta g_{xy0}^{k+1} \tag{22}$$

3) Compute the new buckling factor $\Delta\lambda$ of each unbuckled panel.

The tangent and geometric stiffness matrices at the $k+1$ step is given by

$$K_b = K - e_{x0}^k K^{gx} - e_{y0}^k K^{gy} - g_{xy0}^k K^{gxy} \tag{23}$$

and

$$K^g = \Delta e_{x0}^{k+1} K^{gx} + \Delta e_{y0}^{k+1} K^{gy} + \Delta g_{xy0}^{k+1} K^{gxy} \tag{24}$$

Thus, the buckling equation at the $k+1$ step reduces to

$$K_b \cdot a = \Delta\lambda K^g \cdot a \tag{25}$$

4) Set $\Delta\lambda = 1 - \lambda^k$ for already buckled panels and panels with a negative buckling factor (e.g., panels under tension) . Then the load increment is calculated as

$$\Delta\lambda^k = \min_{\text{all panels}} \Delta\lambda \tag{26}$$

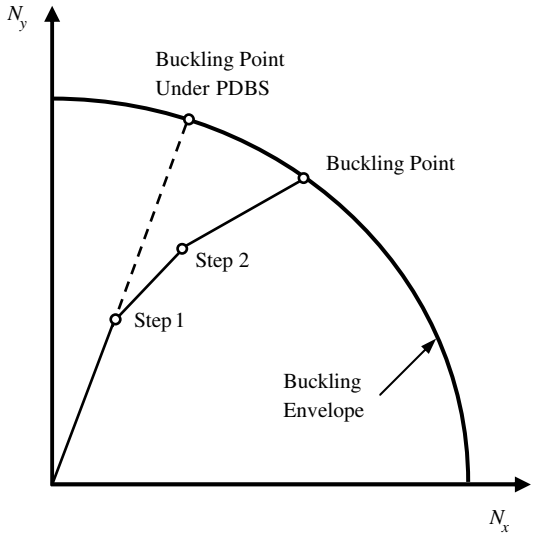

Fig. 2 Schematic diagram of the load history of a typical panel.

5) Update the average strains in all panels according to Eq. (23). Update the load level as $\lambda^{k+1} = \lambda^k + \Delta\lambda^k$.

6) Replace the stiffness of the panel(s) with the lowest buckling factor by the respective postbuckled stiffness.

7) If $\lambda^{k+1} = 1$ then stop, or else set $k = k + 1$ and go to step 2.

From the preceding discussion, it is clear that as soon as a panel buckles a new linear analysis is done by substituting the postbuckled stiffness for the buckled panels. The internal load distribution from this analysis, which may result in changes in both N_x and N_y loadings on the remaining panels, is used to predict buckling factors of the unbuckled panels. Therefore, the biaxial load history of any panel can be shown schematically as in Fig. 2. A simpler alternative is to use the buckling factors computed in the first finite element analysis. This approach is referred to in this paper as a predetermined buckling sequence (PDBS). This approach is exact in loading cases in which the panels are under uniaxial loading because, in essence, we are traversing along one of the axes (refer to Fig. 2). An example that closely approximates uniaxial loading is a wingbox under bending loads.

IV. Results

In this section, we present results obtained for three different problems. First, a single-panel problem subjected to edge displacement compression is used to verify the postbuckled stiffness reduction scheme proposed. Next, a two-panel problem under axial compression is used to demonstrate the iterative scheme. Finally, a wing structure configuration under a bending load is presented. For the purpose of comparison, we also present the full nonlinear analysis results for each case. In all of the example problems, the average loads N_x and N_y are reported. These loads are computed along the displaced edges as follows:

$$N_x = \frac{1}{\underline{b}} \int_0^{\underline{b}} N_x(\underline{a}, y)\, \mathrm{d}y \tag{27}$$

and

$$N_y = \frac{1}{\underline{a}} \int_0^{\underline{a}} N_y(x, \underline{b})\, \mathrm{d}x \tag{28}$$

A. One-Panel Problem

A simply supported square laminate of 10×10 in. dimensions is considered. The material properties are: $E_1 = 18.5 \times 10^6$ psi, $E_2 = 1.6 \times 10^6$ psi, $G_{12} = 0.832 \times 10^6$ psi, $\nu_{12} = 0.35$, and ply thickness $t = 0.005$ in.. Different laminate lay ups and loading conditions are considered, as reported in Table 1. The loading

Table 1 Postbuckling response prediction and comparison for a single composite panel

Laminate lay up	u_0/v_0	λ_{cr}	λ^F	Full analysis N_x, lb/in.	Full analysis N_y, lb/in.	Approx. N_x, lb/in.	Approx. N_y, lb/in.
$[(45\ 90\ -45\ 90)_2]_s$	1/0	2.78	19.93	405.29	−30.11	436.97	−38.41
						436.97	−31.83[a]
$[(0\ 90)_4]_s$	1/0	1.22	13.96	711.51	−294.51	767.58	−303.61[a]
$[\pm 45_4]_s$	1/1	1.0	12.12	317.54	317.54	290.81	290.81
$[(0\ 90)_4]_s$	1/1	0.61	8.29	244.80	239.07	268.96	268.96
$[\pm 45_3\ 90_2]_s$	1.5/1	0.82	9.65	312.62	302.42	323.55	316.17
						321.37	319.42[a]
$[(0\ 90)_4]_s$	1.5/1	0.49	7.02	382.07	119.1	417.31	147.98
						364.46	269.64
$[\pm 45_3\ 90_2]_s$	2/1	0.71	8.18	350.32	254.34	364.46	269.64
						362.62	273.32[a]
$[(0\ 90)_4]_s$	2/1	0.40	6.13	481.29	30.92	529.68	59.31

[a]Results are for a numerical implementation with an averaging of A_{12}^{PB} and A_{21}^{PB} such that $A_{12}^{PB*} = A_{21}^{PB*} = (A_{12}^{PB} + A_{21}^{PB})/2$.

conditions are characterized by the total edge displacement at $x = \underline{a}$ and $y = \underline{b}$ given by u_0 and v_0 (see Table 1). For example, $u_0/v_0 = 1/0$ represents a laminate loaded in uniaxial compression alone, where $u_0 = 1 \times 10^{-3}$ in. and $v_0 = 0$ in.. For $u_0/v_0 = 2/1$, the edge displacement loading is $u_0 = 2 \times 10^{-3}$ in. and $v_0 = 1 \times 10^{-3}$ in.. In all cases, g_{xy0} is assumed to be zero.

In the Rayleigh–Ritz method, we used $N = 9$ ($m = 1, \ldots, 3$ and $n = 1, \ldots, 3$) to predict postbuckled stiffness under the prescribed loading and boundary conditions. The full nonlinear analysis is done using the normal flow algorithm to trace the postbuckled equilibrium [18]. The full nonlinear analysis is also done using $N = 9$. λ^F in Table 1 is the load scaling factor at failure based on initial ply failure taken from Seresta et al. [18]. Therefore, total edge displacement applied at $x = \underline{a}$ is $\lambda^F u_0$ and at $x = \underline{b}$ is $\lambda^F v_0$. In all cases, the edge displacement applied is more than 10 times that of the critical or buckling factor λ_{cr}.

From Table 1, we observe that for all the laminate stacking sequences and edge displacement loading conditions considered the proposed approximate methodology predicts the average panel loads within reasonable margins. The maximum relative error in the predicted value of N_x is 10%. In some cases, the relative error in the predicted values of N_y is large (up to to nearly 100%). This occurs only when the N_x/N_y ratio is large. For example, in the case of laminate lay up $[(0\ 90)_4]_s$ with edge displacement loading ratio 2, the error in N_y prediction is significant but the N_x/N_y ratio is greater than 15. Thus, the primary load is along the x direction. It can be seen that large relative errors in the predicted average loads occur only along the secondary loading direction and are not significant for design purposes.

In some cases, two values of the approximate average loads are reported in Table 1. In such cases, the difference in the numerically computed postbuckled stiffness coefficients A_{12}^{PB} and A_{21}^{PB} is large enough to be observable. It can be seen that the difference between the loads computed based on the averaged value of A_{12}^{PB} and A_{21}^{PB} (reported in bold) agrees well with the values computed without averaging. Thus, the symmetrized postbuckled stiffness can be used for all computations, which is essential for the approximate methodology to be compatible with commercially available finite element codes.

Note that in the current example problem, no finite element analysis is done and the error reported is only because of the approximation in postbuckled stiffness formulation. In the next example, we will observe another source of error.

B. Two-Panel Problem

A two-panel composite structure as shown in Fig. 3 is considered next. Each panel, P1 and P2 ($a \times b$ in Fig. 3), has dimensions of 10×10 in.. The material properties and ply thickness are the same as in the previous example. The boundary conditions and the edge displacement loading conditions are shown in Fig. 3. L1, B1, T1, and R1 in Fig. 3 refer to the left, bottom, top, and right edges of panel P1, respectively. Similarly, L2, B2, T2, and R2 refer to the left, bottom, top, and right edges of panel P2, respectively. Both P1 and P2 are simply supported and edge displacement $2e_{x0}a$ is applied to R2 (see Fig. 3). Edge displacement $e_{y0}b$ is applied at T1 and T2 (see Fig. 3).

The laminate stacking sequence for panels P1 and P2 are $[(0\ 90)_8]_s$ and $[(0\ 90)_4]_s$, respectively. In the Rayleigh–Ritz method, we used $N = 25$ ($m = 1, 2, \ldots, 5$ and $n = 1, 2, \ldots, 5$) to predict the postbuckled stiffness of the individual laminate. In this example problem, the proposed methodology is implemented using the commercially available finite element package NASTRAN [35]. For the purpose of comparison, we report both the full nonlinear finite element analysis and the approximate analysis results in Table 2. Both the linear and nonlinear analyses are done using a mesh of 10×10 CQUAD4 [35] elements for each panel.

The panel loads predicted by the proposed scheme are compared with a full nonlinear analysis at five different stages of loading, as reported in Table 2. The buckling factors for P1 and P2 are also reported at the beginning of Table 2.

In load stage 1, only P2 has buckled (see Fig. 4). The maximum relative error in edge load prediction for P1 is 15% at R1 and for P2 is 26% at R2. The maximum error for P1 occurs at the edge it shares with the buckled P2 panel. In load stage 2, once again only P2 has buckled. The maximum error for P1 is 17% at R1 and for P2 is 21% at R2. In load stage 3, both P1 and P2 have buckled but the loading condition is such that P1 is closer to its buckling load. The maximum error for P1 is 11.4% at R1 and for P2 is 17.66% at R2. In load stage 4, both P1 and P2 are deep into the postbuckling regime. The total loading is 1.5 times that of the buckling load for P1 and 8 times that of the buckling load of P2. The maximum error for P1 is 16.47% at R1 and for P2 is 23.4% at L2. In load stage 5, the total loading for P1 is 3.1 times that of its buckling load and for P2 is 16.4 times that of its buckling load. The maximum error for P1 is 21.21% at L1 and for P2 is 15.82% at L2. The postbuckled configuration of the structure at load stage 5 is shown in Fig. 5.

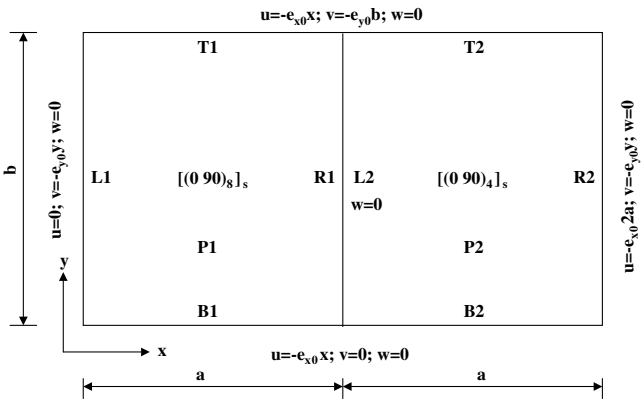

Fig. 3 Two-panel (P1 and P2) composite structure showing edges (L1, B1, T1, R1 of P1 and L2, B2, T2, R2 of P2), boundary conditions, and lay ups.

Table 2 Postbuckling response of a two-panel composite structure (P1: $\frac{u_0}{v_0} = \frac{0.001}{0.002}$, $\lambda_{cr} = 1.62$; P2: $\frac{u_0}{v_0} = \frac{0.002}{0.002}$, $\lambda_{cr} = 0.304$

Load stage 1: $u_0 = 0.002$ in., $v_0 = 0.002$ in.								
Analysis	L1	B1	T1	R1	L2	B2	T2	R2
	N_x, lb/in.	N_y, lb/in.	N_y, lb/in.	N_x, lb/in.	N_x, lb/in.	N_y, lb/in.	N_y, lb/in.	N_x,lb/in.
Full NL	123.0	326.9	326.9	96.45	86.06	127.8	127.8	70.45
Approx.	117.2	329.2	327.4	81.85	67.61	100.4	99.87	52.1
Rel. error	4.65	−0.72	−0.17	15.13	21.44	21.46	21.87	26.05
Load stage 2: $u_0 = 0.0025$ in., $v_0 = 0.0025$ in.								
Analysis	L1	B1	T1	R1	L2	B2	T2	R2
Full NL	146.2	406.4	402.5	118.0	96.06	145.9	144.0	73.96
Approx.	143.2	410.6	412.2	97.57	77.31	117.9	118.5	58.32
Rel. error	2.05	−1.03	−2.4	17.31	19.52	19.23	17.71	21.15
Load stage 3: $u_0 = 0.0033$ in., $v_0 = 0.0033$ in.								
Analysis	L1	B1	T1	R1	L2	B2	T2	R2
Full NL	179.5	526.3	523.2	133.4	108.9	172.4	170.9	78.59
Approx.	182.0	533.4	528.6	118.2	94.01	146.9	145.3	64.71
Rel. error	−1.35	−1.35	−1.04	11.4	13.7	14.77	14.97	17.66
Load stage 4: $u_0 = 0.005$ in., $v_0 = 0.005$ in.								
Analysis	L1	B1	T1	R1	L2	B2	T2	R2
Full NL	216.3	714.4	714.4	145.9	127.3	228.0	228.0	84.58
Approx.	185.5	670.8	668.2	121.9	97.53	214.6	214.0	69.82
Rel. error	14.26	6.09	6.46	16.47	23.4	5.9	6.16	17.45
Load stage 5: $u_0 = 0.01$ in., $v_0 = 0.01$ in.								
Analysis	L1	B1	T1	R1	L2	B2	T2	R2
Full NL	254.3	1117.2	1117.2	172.0	128.2	402.5	402.5	82.21
Approx.	200.4	1073.3	1070.2	137.2	107.9	414.7	413.9	81.76
Rel. error	21.21	3.93	4.21	20.22	15.82	3.01	2.81	0.55

In general, for all the load steps it is found that the approximate scheme gives reasonably good results and the maximum error is about 20%. Note that the buckling factors are computed assuming simply supported boundary conditions, but at R1 and L2 there should be slope continuity, which the local model cannot capture thus introducing further errors. It is observed that the relative error does not change appreciably from load stage 1 to 3 when only P2 has buckled. This indicates that a substantial percentage of the error is due to the error in the buckling factor, because the errors due to the linear postbuckling approximation grow as the panel goes deeper in the postbuckling regime, as shown in the one-panel problem. Thus, errors due to the approximation and due to the underpredicted buckling factor seem to grow in different directions, keeping the total error relatively constant.

C. Forty-Eight Panel Composite Wingbox Problem

In this example, we analyze a large tapered rectangular composite wingbox $160 \times 30 \times 4$ ft (root)/2.4 ft (tip), as shown in Fig. 6. The wingbox is divided into 24 upper skin panels and 24 bottom skin panels by longitudinal spars and transverse ribs. All of the top and bottom skin panels are 20×10 ft in dimension. The material properties and the ply thickness are the same as in the earlier examples. The root of the wing is fixed. A total of 3100 lb upward load is applied at the free end and uniformly distributed among nodes at the top edge of the free end. Each of the top and bottom skin panels is modeled using 200 CQUAD4 elements for nonlinear finite element analysis using NASTRAN. The total number of elements in the model is 13,120. In the approximate analysis and linear analysis, the number of elements per panel is one. The total number of elements in the proposed approximate model is only 104.

The wingbox panels are divided into three regions (see Fig. 6): root (panels 1–9), intermediate (panels 9–18), and free end or tip (panels 18–24). All of the top skin root panels are made of $[(0\ 90)_{40}]_s$, the bottom skin root panels are made of $[(0\ 90)_{25}]_s$, the spar root panels are made of $[(0\ 90)_{50}]_s$, and the rib root panels are made of $[(0\ 90)_{50}]_s$. All of the top skin intermediate panels are made of $[(0\ 90)_{20}]_s$, the bottom skin intermediate panels are made of $[(0\ 90)_{15}]_s$, the spar intermediate panels are made of $[(0\ 90)_{50}]_s$, and the rib intermediate panels are made of $[(0\ 90)_{50}]_s$. All of the top skin free-end or tip panels are made of $[(0\ 90)_{10}]_s$, the bottom skin free-end or tip panels are made of $[(0\ 90)_5]_s$, the spar free-end or tip panels

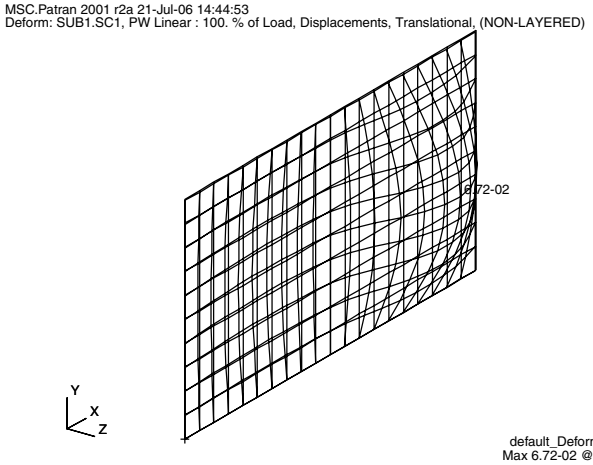

Fig. 4 Buckled configuration from a nonlinear finite element analysis at load stage 1.

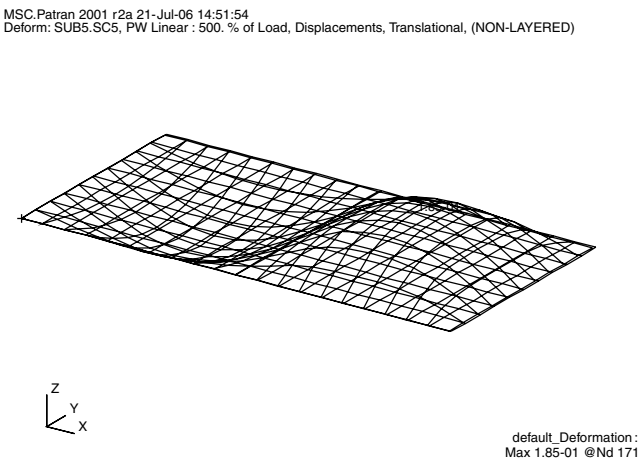

Fig. 5 Buckled configuration from a nonlinear finite element analysis at load stage 5.

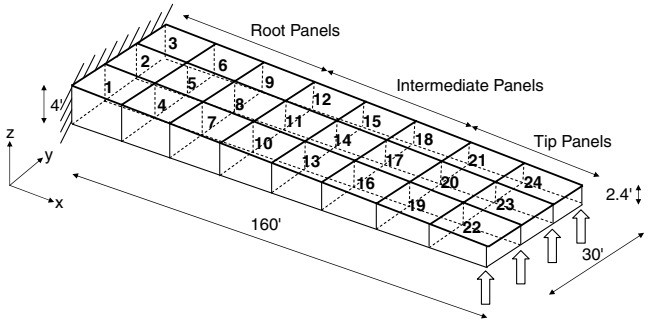

Fig. 6 Wingbox configuration.

are made of $[(0\ 90)_{50}]_s$, and the rib free-end or tip panels are made of $[(0\ 90)_{50}]_s$. The spar and rib panels in this model are too thick to allow the free rotation of edges, but this is necessary to avoid the buckling of spars and ribs under the load. This is done to facilitate the interpretation of results, and we chose to focus mainly on the skin panels. In the Rayleigh–Ritz method, we used $N = 25$ to compute the postbuckled stiffness.

For the purpose of comparison, we present the internal load distribution in the structure for the full nonlinear analysis, the linear analysis, the approximate analysis, and the approximate analysis with PDBS in Table 3. The average loads reported are taken at the midsection of each panel, because the loads model for both the linear and approximate analyses has only one element per panel. Only top skin panels are reported, as they are the ones under compression and susceptible to buckling. The linear analysis overpredicts the average loads by 26% (see Table 3). Compared with the linear analysis, the approximate analysis performs much better, only overpredicting the loads by 3% (see 3). From the postbuckled configuration of the wingbox (Fig. 7), we see that panels 19, 20, and 21 have buckled under the applied loads. In the approximate internal load prediction scheme, the local analysis of panels 10–18 predicts them buckled. As mentioned earlier, this local analysis is based on the assumption that the panel is simply supported and flat. The predicted buckling loads of panels 10–18 will be underpredicted because of the idealized boundary conditions. It is difficult to ascertain whether these panels are buckled or not from the nonlinear analysis results. This is because

Table 3 Postbuckling response in the top skin of a 48-panel composite wing structure

Panel no.	Full NL N_x, lb/ft	Linear N_x, lb/ft	Approx. N_x, lb/ft	Approx. PDBS N_x, lb/ft
1	3724.1	3734.3	3733.6	3733.6
2	3707.8	3711.4	3712.7	3712.8
3	3724.1	3734.3	3733.6	3733.6
4	3415.4	3419.5	3420.1	3420.2
5	3400.1	3411	3408.8	3408.7
6	3415.3	3419.5	3420.1	3420.2
7	3059.4	3080	3098.5	3099.3
8	3026.5	3037.3	2998.8	2997.2
9	3059.5	3080	3098.5	3099.3
10	2446.6	2445.1	2220.2[a]	2211.9[a]
11	2456.6	2463.8	2259.5[a]	2252.2[a]
12	2446.3	2445.1	2220.2[a]	2211.9[a]
13	2037	2044.3	1867.7[a]	1860.6[a]
14	2032.4	2044.9	1880.2[a]	1874.3[a]
15	2036.9	2044.3	1867.7[a]	1860.6[a]
16	1539	1578.1	1490.2[a]	1493.3[a]
17	1515.9	1556.9	1439.1[a]	1440.2[a]
18	1539	1578.1	1490.2[a]	1493.3[a]
19	757.01[a]	954.71	784.67[a]	784.74[a]
20	782.95[a]	945.37	794.46[a]	794.89[a]
21	757.01[a]	954.71	784.67[a]	784.74[a]
22	309.76	346.15	286.48	292.72
23	306.1	323.63	271.91	277.14
24	306.38	346.15	286.48	292.71

[a]Indicates the buckled panels.

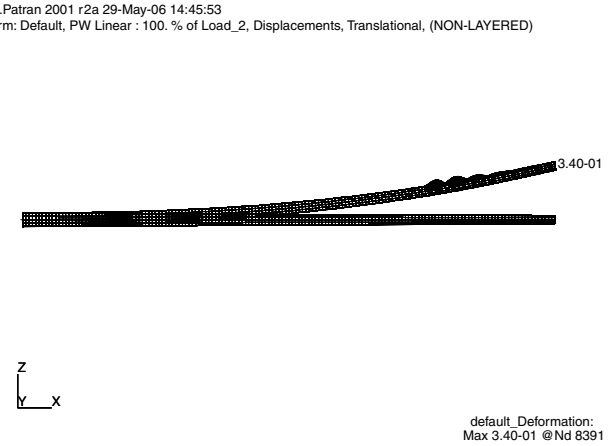

Fig. 7 Deformed wingbox configuration from a nonlinear finite element analysis under the total applied load.

flat plates have a stable postbuckling response and in the initial buckling stage they do not show much deformation. Because the approximate model assumes a simply supported flat panel, the resultant design will always be conservative in nature. It can also be seen that approximate analysis with a predetermined buckling sequence is also in good agreement. This is because in the present example the panels are mostly uniaxially loaded.

V. Conclusions

In this paper, we developed a methodology to predict the internal load distribution in postbuckled composite structures. The proposed scheme is a progressive buckling analysis in which the stiffness of a buckled component is replaced by its postbuckled stiffness for load levels above its buckling capacity. A new semi-analytical method based on the Rayleigh–Ritz method is presented to compute the postbuckled stiffness.

The proposed scheme is demonstrated via three different problems. For all of the problems, idealized simply supported boundary conditions are used for the prediction of the postbuckled stiffness. First, a single panel subjected to both uniaxial and biaxial edge displacement is analyzed. The analysis result showed that the proposed scheme predicts the average loads well. It is also observed that sometimes the reduced stiffness coefficient matrix is not symmetric, but the difference is very small and can be reasonably averaged for application along with commercial finite element packages. Second, a two-panel structure subjected to biaxial edge displacement is analyzed. In this case also, the panel responses are predicted with reasonable confidence. The results indicate the importance of accurate local models in predicting the buckling factor and postbuckled stiffness. Refining the local model to reflect the actual panel boundary conditions in an assembled structure is an area where further research is needed. A possible solution is to introduce edge torsional stiffness estimated from a global analysis of the structure. However, it is noteworthy that simply supported boundary conditions lead to conservative load estimates and are a standard idealization in any multilevel design of large composite structures, such as an aircraft fuselage or a wingbox. Third, a 48-panel composite wing structure subjected to bending load is analyzed and reasonable accuracy is demonstrated.

Based on the example problems solved, it can be concluded that the proposed methodology can be applied as a loads model in the multilevel design optimization of a large structure at the preliminary design stages when local buckling of some or all of the structural subcomponents is allowed. This would be computationally intractable otherwise, because of expensive full nonlinear analysis. The proposed scheme presents a systematic approach to passing on the local information to a global model without needing to refine the finite element model.

Appendix A: Full Form of the Tensors

The full forms of the tensors appearing in system of Eqs. (7) are as follows:

$$g_l^{ux} = \int_0^{\underline{a}} \int_0^{\underline{b}} A_{11}\phi_{l,x}^u \,\mathrm{d}x\,\mathrm{d}y$$

$$g_l^{uy} = \int_0^{\underline{a}} \int_0^{\underline{b}} A_{12}\phi_{l,x}^u \,\mathrm{d}x\,\mathrm{d}y$$

$$g_l^{uxy} = \int_0^{\underline{a}} \int_0^{\underline{b}} A_{66}\phi_{l,y}^u \,\mathrm{d}x\,\mathrm{d}y$$

$$g_l^{vx} = \int_0^{\underline{a}} \int_0^{\underline{b}} A_{12}\phi_{l,y}^v \,\mathrm{d}x\,\mathrm{d}y$$

$$g_l^{vy} = \int_0^{\underline{a}} \int_0^{\underline{b}} A_{22}\phi_{l,y}^v \,\mathrm{d}x\,\mathrm{d}y$$

$$g_l^{vxy} = \int_0^{\underline{a}} \int_0^{\underline{b}} A_{66}\phi_{l,x}^v \,\mathrm{d}x\,\mathrm{d}y$$

$$K_{il}^{ub} = \int_0^{\underline{a}} \int_0^{\underline{b}} [A_{11}\phi_{i,x}^u\phi_{l,x}^u + A_{66}\phi_{i,y}^u\phi_{l,y}^u]\,\mathrm{d}x\,\mathrm{d}y$$

$$K_{il}^{uc} = \int_0^{\underline{a}} \int_0^{\underline{b}} [A_{12}\phi_{i,y}^v\phi_{l,x}^u + A_{66}\phi_{i,x}^v\phi_{l,y}^u]\,\mathrm{d}x\,\mathrm{d}y$$

$$K_{ijl}^{ua} = \frac{1}{2}\int_0^{\underline{a}} \int_0^{\underline{b}} [A_{11}\phi_{i,x}^w\phi_{j,x}^w\phi_{l,x}^u + A_{12}\phi_{i,y}^w\phi_{j,y}^w\phi_{i,x}^u + A_{66}\phi_{i,x}^w\phi_{j,y}^w\phi_{l,y}^u + A_{66}\phi_{i,y}^w\phi_{j,x}^w\phi_{l,y}^u]\,\mathrm{d}x\,\mathrm{d}y$$

$$K_{il}^{vb} = \int_0^{\underline{a}} \int_0^{\underline{b}} [A_{12}\phi_{i,x}^u\phi_{l,y}^v + A_{66}\phi_{i,y}^u\phi_{l,x}^v]\,\mathrm{d}x\,\mathrm{d}y$$

$$K_{il}^{vc} = \int_0^{\underline{a}} \int_0^{\underline{b}} [A_{22}\phi_{i,y}^v\phi_{l,y}^v + A_{66}\phi_{i,x}^v\phi_{l,x}^v]\,\mathrm{d}x\,\mathrm{d}y$$

$$K_{ijl}^{va} = \frac{1}{2}\int_0^{\underline{a}} \int_0^{\underline{b}} [A_{12}\phi_{i,x}^w\phi_{j,x}^w\phi_{l,y}^v + A_{22}\phi_{i,y}^w\phi_{j,y}^w\phi_{l,y}^v + A_{66}\phi_{i,x}^w\phi_{j,y}^w\phi_{l,x}^v + A_{66}\phi_{i,y}^w\phi_{j,x}^w\phi_{l,x}^v]\,\mathrm{d}x\,\mathrm{d}y$$

$$\bar{K}_{il} = \int_0^{\underline{a}} \int_0^{\underline{b}} [D_{11}\phi_{i,xx}^w\phi_{l,xx}^w + D_{12}\phi_{i,yy}^w\phi_{l,xx}^w + D_{12}\phi_{i,xx}^w\phi_{l,yy}^w + D_{22}\phi_{i,yy}^w\phi_{l,yy}^w + 4D_{66}\phi_{i,xy}^w\phi_{l,xy}^w]\,\mathrm{d}x\,\mathrm{d}y$$

$$\bar{K}_{il}^{gx} = \int_0^{\underline{a}} \int_0^{\underline{b}} [A_{11}\phi_{i,x}^w\phi_{l,x}^w + A_{12}\phi_{i,y}^w\phi_{l,x}^w]\,\mathrm{d}x\,\mathrm{d}y$$

$$\bar{K}_{il}^{gy} = \int_0^{\underline{a}} \int_0^{\underline{b}} [A_{12}\phi_{i,x}^w\phi_{l,x}^w + A_{22}\phi_{i,y}^w\phi_{l,x}^w]\,\mathrm{d}x\,\mathrm{d}y$$

$$\bar{K}_{il}^{gxy} = \int_0^{\underline{a}} \int_0^{\underline{b}} [A_{66}\phi_{i,y}^w\phi_{l,x}^w + A_{66}\phi_{i,x}^w\phi_{l,y}^w]\,\mathrm{d}x\,\mathrm{d}y$$

$$K_{ikl}^{wba} = \int_0^{\underline{a}} \int_0^{\underline{b}} [A_{11}\phi_{i,x}^u\phi_{k,x}^w\phi_{l,x}^w + A_{12}\phi_{i,x}^u\phi_{k,y}^w\phi_{l,y}^w + A_{66}\phi_{i,y}^u\phi_{k,y}^w\phi_{l,x}^w + A_{66}\phi_{i,y}^u\phi_{k,x}^w\phi_{l,y}^w]\,\mathrm{d}x\,\mathrm{d}y$$

$$K_{ikl}^{wca} = \int_0^{\underline{a}} \int_0^{\underline{b}} [A_{12}\phi_{i,y}^v\phi_{k,x}^w\phi_{l,x}^w + A_{22}\phi_{i,y}^v\phi_{k,y}^w\phi_{l,y}^w + A_{66}\phi_{i,x}^v\phi_{k,y}^w\phi_{l,x}^w + A_{66}\phi_{i,x}^v\phi_{k,x}^w\phi_{l,y}^w]\,\mathrm{d}x\,\mathrm{d}y$$

$$\begin{aligned}\bar{K}_{ijkl}^{waa} = \frac{1}{2}\int_0^{\underline{a}} \int_0^{\underline{b}} [&A_{11}\phi_{i,x}^w\phi_{j,x}^w\phi_{k,x}^w\phi_{l,x}^w + A_{12}\phi_{i,y}^w\phi_{j,y}^w\phi_{k,x}^w\phi_{l,x}^w \\ &+ A_{12}\phi_{i,x}^w\phi_{j,x}^w\phi_{k,y}^w\phi_{l,y}^w + A_{22}\phi_{i,y}^w\phi_{j,y}^w\phi_{k,y}^w\phi_{l,y}^w \\ &+ A_{66}\phi_{i,x}^w\phi_{j,y}^w\phi_{k,y}^w\phi_{l,x}^w + A_{66}\phi_{i,x}^w\phi_{j,y}^w\phi_{k,x}^w\phi_{l,y}^w \\ &+ A_{66}\phi_{i,y}^w\phi_{j,x}^w\phi_{k,y}^w\phi_{l,x}^w + A_{66}\phi_{i,y}^w\phi_{j,x}^w\phi_{k,x}^w\phi_{l,y}^w]\,\mathrm{d}x\,\mathrm{d}y\end{aligned}$$

Appendix B: Condensation Procedure

The condensation procedure involves the readjusting and reordering of the tensors in the following manners:

$$\{\boldsymbol{e}\} = \begin{Bmatrix}\{\boldsymbol{b}\}\\ \{\boldsymbol{c}\}\end{Bmatrix}$$

$$\{\boldsymbol{g}\} = \begin{Bmatrix}\{\boldsymbol{g}^u\}\\ \{\boldsymbol{g}^v\}\end{Bmatrix}$$

$$[\boldsymbol{K}^a] = \begin{bmatrix}[\boldsymbol{K}^{ub}] & [\boldsymbol{K}^{uc}]\\ [\boldsymbol{K}^{vb}] & [\boldsymbol{K}^{vc}]\end{bmatrix}$$

$$K_{ijp}^{ab} = \begin{cases} K_{ijl}^{uaa} & \text{for } p = 1, 2, 3, \ldots, 2n \\ K_{ijl}^{vaa} & \text{for } p = 2n+1, \ldots, 4n \end{cases}$$

and

$$K_{pkl}^{ba} = \begin{cases} K_{ikl}^{wba} & \text{for } p = 1, 2, 3, \ldots, 2n \\ K_{ikl}^{wca} & \text{for } p = 2n+1, \ldots, 4n \end{cases}$$

Then, e_p is given as

$$e_p = \lambda^T(K_{pl}^{-a} g_l) - K_{ps}^{-a}K_{ijs}^{ab}a_i a_j = \lambda^T h_p - K_{ps}^{-a}K_{ijs}^{ab}a_i a_j$$

Substituting e_p in the last equation of Eq. (7), we the get following equation:

$$K_{il}a_i - \lambda^T\bar{K}_{il}^g a_i + K_{pkl}^{ba}(\lambda^T h_p - K_{ps}^{-a}K_{ijs}^{ab}a_i a_j)a_k + K_{ijkl}^{waaa}a_i a_j a_k = 0$$

Rearranging the terms in the preceding equation, we get the final equation as follows:

$$[K_{il} - \lambda^T(\bar{K}_{il}^g - K_{pil}^{ba}h_p)]a_i + (K_{ijkl}^{waaa} - K_{pkl}^{ba}K_{ps}^{-a}K_{ijs}^{ab})a_i a_j a_k = 0,$$

$$\text{or } [K_{il} - \lambda^T K_{il}^g]a_i + K_{ijkl}^{\mathrm{NL}}a_i a_j a_k = 0$$

Acknowledgments

The authors would like to acknowledge the effort of the reviewers and their invaluable and detailed suggestions to make the paper organized and lucid.

References

[1] Lansing, W., Dwyer, W., Emerton, R., and Ranalli, E., "Application of Fully Stressed Design Procedures to Wing and Empennage Structures," *Journal of Aircraft*, Vol. 8, No. 9, 1971, pp. 683–688.

[2] Giles, G. L., "Procedure for Automating Aircraft Wing Structural Design," *Journal of the Structural Division*, Vol. 97, No. 1, 1971, pp. 99–113.

[3] Sobieszczanski-Sobieski, J., and Leondorf, D., "A Mixed Optimization Method for Automated Design of Fuselage Structures," *Journal of Aircraft*, Vol. 9, No. 12, 1972, pp. 805–811.

[4] Schmit, L. A., and Ramanathan, R. K., "Multilevel Approach to Minimum Weight Design Including Buckling Constraints," *AIAA Journal*, Vol. 16, No. 2, 1978, pp. 97–104.

[5] Schmit, L. A., and Mehrinfar, M., "Multilevel Optimum Design of Structures with Fiber Composite Stiffened Panel Components," *AIAA Journal*, Vol. 20, No. 1, 1982, pp. 138–147.

[6] Sobieszczanski-Sobieski, J., James, B. B., and Dovi, A. R., "Structural Optimization by Multilevel Decomposition," *AIAA Journal*, Vol. 23, No. 11, 1985, pp. 1775–1782.

[7] Sobieszczanski-Sobieski, J., James, B. B., and Riley, M. F., "Structural Sizing by Generalized Multilevel Optimization," *AIAA Journal*, Vol. 25, No. 1, 1987, pp. 139–145.

[8] Ragon, S. A., Gürdal, Z., Haftka, R. T., and Tzong, T. J., "Bilevel Design of Wing Structure using Response Surfaces," *Journal of Aircraft*, Vol. 40, No. 5, 2003, pp. 985–992.

[9] Liu, B., Haftka, R. T., and Akgün, M. A., "Two-Level Composite Wing Structural Optimization Using Response Surfaces," *Structural and Multidisciplinary Optimization*, Vol. 20, No. 2, 2000, pp. 87–96. doi:10.1007/s001580050140

[10] Nagendra, S., Haftka, R. T., and Gürdal, Z., "Stacking Sequence Optimization of Simply Supported Laminates with Stability and Strain Constraints," *AIAA Journal*, Vol. 30, No. 8, 1992, pp. 2132–2137.

[11] Riche, R. L., and Haftka, R. T., "Optimization of Stacking Sequence Design for Buckling Load Maximization Using Genetic Algorithm," *AIAA Journal*, Vol. 31, No. 5, 1993, pp. 951–956.

[12] Miki, M., and Sugiyama, Y., "Optimum Design of Laminated Composite Plates Using Lamination Parameters," *AIAA Journal*, Vol. 31, No. 5, 1993, pp. 921–922.

[13] Kogiso, N., Watson, L. T., Gürdal, Z., and Haftka, R. T., "Genetic Algorithms with Local Improvement for Composite Laminate Design," *Structural Optimization*, Vol. 7, No. 4, 1994, pp. 207–218. doi:10.1007/BF01743714

[14] Soremekun, G., Gürdal, Z., Haftka, R. T., and Watson, L. T., "Composite Laminate Design Optimization by Genetic Algorithm with Generalized Elitist Selection," *Computers and Structures*, Vol. 79, No. 2, 2001, pp. 131–143. doi:10.1016/S0045-7949(00)00125-5

[15] McMahon, M. T., Watson, L. T., Soremekun, G., Gürdal, Z., and Haftka, R. T., "A Fortran 90 Genetic Algorithm Module for Composite Laminate Structure Design," *Engineering with Computers*, Vol. 14, No. 3, 1998, pp. 260–273. doi:10.1007/BF01215979

[16] Perry, A. C., Gürdal, Z., and Starnes, J. H. Jr., "Minimum-Weight Design of Compressively Loaded Stiffened Panels for Postbuckling Response," *Engineering Optimization*, Vol. 28, No. 3, 1997, pp. 175–197. doi:10.1080/03052159708941131

[17] Shin, D. K., Gürdal, Z., and Griffin, O. H., "Minimum Weight Design of Laminated Composite Plates for Postbuckling Performance," *Proceedings of the 32nd AIAA/ASME/ASCE/AHS/ASC Structures, Structural Dynamics and Materials Conference*, AIAA, Washington, D.C., April 1991, pp. 257–262.

[18] Seresta, O., Abdalla, M. M., and Gürdal, Z., "Optimal Design of Laminated Composite Plates for Maximum Postbuckling Strength," *Proceedings of the 46th AIAA/ASME/ASCE/AHS/ASC Structures, Structural Dynamics, and Materials Conference*, AIAA, Reston, VA, April 2005.

[19] Adali, S., Walker, M., and Verijenko, V. E., "Multiobjective Optimization of Laminated Plates for Maximum Prebuckling, Buckling and Postbuckling Strength Using Continuous and Discrete Ply Angles," *Composite Structures*, Vol. 35, No. 1, 1996, pp. 117–130. doi:10.1016/0263-8223(96)00030-X

[20] Diaconu, C. G., and Weaver, P. M., "Approximate Solution and Optimum Design of Compression Loaded, Postbuckled Laminated Composite Plates," *AIAA Journal*, Vol. 43, No. 4, 2005, pp. 906–914.

[21] Grisham, A. F., "A Method for Including Postbuckling of Plate Elements in the Internal Load Analysis of Any Complex Structure Idealized Using Finite Element Analysis Methods," *Proceedings of the 19th Structures, Structural Dynamics, and Materials Conference*, AIAA, New York, April 1978, pp. 359–369.

[22] Williams, F. W., Kennedy, D., Butler, R., and Anderson, M. S., "VICONOPT: Program for Exact Vibration and Buckling Analysis or Design of Prismatic Plate Assemblies," *AIAA Journal*, Vol. 29, No. 11, 1991, pp. 1927–1928.

[23] Anderson, M. S., "Design of Panels having Postbuckling Strength," *Proceedings of the 38th AIAA/ ASME/ASCE/AHS/ASC Structures, Structural Dynamics, and Materials Conference*, AIAA, Reston, VA, April 1997, pp. 2407–2413.

[24] Viljoen, A., Visser, A. G., and Groenwold, A. A., "Computationally Efficient Analysis and Optimization of Stiffened Thin-Walled Panels in Shear," *Journal of Aircraft*, Vol. 42, No. 3, 2005, pp. 743–747.

[25] Collier, C., Yarrington, P., and West, B. V., "Composite, Grid-Stiffened Panel Design for Post Buckling using Hypersizer," *Proceedings of the 43rd AIAA/ASME/ASCE/AHS/ASC Structures, Structural Dynamics, and Materials Conference*, AIAA, Reston, VA, April 2002, pp. 1–16.

[26] Haftka, R. T., "Damage Tolerant Design Using Collapse Techniques," *AIAA Journal*, Vol. 21, No. 10, 1983, pp. 1462–1466.

[27] Rikards, R., Abramovich, H., Kalnins, K., and Auzins, J., "Surrogate Modeling in Design Optimization of Stiffened Composite Shells," *Composite Structures*, Vol. 73, No. 2, 2006, pp. 244–251. doi:10.1016/j.compstruct.2005.11.046

[28] Lanzi, L., and Giavotto, V., "Postbuckling Optimization of Composite Stiffened Panels: Computations and Experiments," *Composite Structures*, Vol. 73, No. 2, 2006, pp. 208–220. doi:10.1016/j.compstruct.2005.11.047

[29] Murphy, A., Price, M., Gibson, A., and Armstrong, C. G., "Efficient Nonlinear Idealisations of Aircraft Fuselage Panels in Compression," *Finite Elements in Analysis and Design*, Vol. 40, Nos. 13–14, 2004, pp. 1977–1993. doi:10.1016/j.finel.2003.11.009

[30] Kling, A., Degenhardt, R., and Zimmermann, R., "A Hybrid Subspace Analysis Procedure for Nonlinear Postbuckling Calculation," *Composite Structures*, Vol. 73, No. 2, 2006, pp. 162–170. doi:10.1016/j.compstruct.2005.11.051

[31] Turvey, G. J., and Marshall, I. H., *Buckling and Postbuckling of Composite Plates*, Chapman and Hall, London, 1995.

[32] Whitney, J. M., *Structural Analysis of Laminated Anisotropic Plates*, Technomic, Lancaster, PA, 1987.

[33] Lekhintskii, S. G., *Anisotropic Plates*, Translated by S. W. Tsai and C. T. Gordon, Breach Science Publishers, Inc., 1968.

[34] Shin, D. K. Jr., O. H. G., and Gürdal, Z., "Postbuckling Response of Laminated Plates Under Uniaxial Compression," *International Journal of Non-Linear Mechanics*, Vol. 28, No. 1, 1993, pp. 95–115. doi:10.1016/0020-7462(93)90009-A

[35] Kilroy, K., *Nastran Manual*, The MacNeal-Schwendler Corporation, Los Angeles, 1995.